Use of high spatial resolution distributed optical fiber to monitor the crack propagation of an adhesively bonded joint during ENF and DCB tests

Quentin Sourisseau, Emilie Leprêtre, Sylvain Chataigner, Xavier Chapeleau, Luc Mouton, Stéphane Paboeuf

Use of high spatial resolution distributed optical fiber to monitor the crack propagation of an adhesively bonded joint during ENF and DCB tests.

Quentin Sourisseau [1, 2, 3], Emilie Lepretre [1], Sylvain Chataigner [1], Xavier Chapeleau [2], Luc Mouton [3], Stéphane Paboeuf [3]

[1], *University Gustave Eiffel, MAST-SMC Bouguenais, France,* [2] *University Gustave Eiffel, Inria, COSYS-SII, I4S Team, Bouguenais, France,* [3] *Bureau Veritas Marine & Offshore, Environment & Technologies Department, Nantes, France*

Abstract:

Similarly to other industrial areas, there is a strong interest for the use of bonded FRP (Fiber Reinforced Polymers) repair or reinforcement for steel structures in the case of offshore applications. However, the reliability of the adhesively bonded (FRP) shall stand as high as steel renewal, this requires additional developments, in particular, a complete understanding of the repair mechanical strength which depends on material and interfacial properties. Fracture mechanics is an interesting approach to assess the risk to undergo interlaminar fracture or steel to adhesive interfacial disbonding failure. The experimental determination of the required design values for this an approach (critical toughness) are generally obtained using common tests such as Double Cantilever Beam (DCB), End Notched Flexure (ENF) or Mixed Mode Bending (MMB) tests. These tests require a precise crack length monitoring that is currently carried out using visual observation or Digital Image Correlation (DIC) on the flank of the sample. This may induce error in crack length measurement especially if the crack doesn't remain straight during the test. The paper presents a study of crack front monitoring by a distributed optical fiber as an alternative to the standard techniques to monitor crack front and to determine the critical toughness in mode I and II through respectively, DCB (Double Cantilever Beam) and ENF (End Notched Flexure) tests. Firstly, the issues related to the use of this continuous optical fiber are raised (insertion, precision resolution, measurement noise, exploitation methodologies). Then, some experimental investigations on ENF and DCB tests are presented and analyzed using the proposed methodology to monitor crack propagation using the optical fiber strain measurement. The obtained results are compared, focusing on the proper determination of the critical toughness of the adhesive. These results show that an optical fiber bonded on the surface of the sample can be used to measure and follow the crack propagation during the test which simplifies and adds precision to the standardize critical toughness computation method.

1. Introduction:

The maintenance of marine steel structures installed in harsh offshore environment (like tropical areas) is a great challenge. Vessels and mobile offshore units can be maintained and repaired onshore in shipyards, units such as Floating Production Storage and Offloading platforms (FPSO) are permanently moored at sea and shall be maintained on site. Similarly, naval ships may also be faced with the need to perform repairs in short period of time at sea to maintain operability. On FPSO units, the corrosion is a

permanent threat due to high temperature and high humidity conditions. Bonded repair solutions which present several advantages (short down-time and non-intrusively process) are actually in development. However, repairing corroded areas on large marine structures by bonding FRP patch imposes important constraints on the design. The patch lies in fully stressed area (for instance area subject to hull girder flexibility), causing high stresses in the bond line edges. Designers and engineers face several difficulties related to the nature of hybrid steel to composite joints:

- Materials discontinuity (material properties),
- Nonlinear material properties of the adhesive,
- Singularity at the edge of the patch.

Thus, a fine apprehension of adhesion mechanics and strength is critical for designing highly reliable composite patch repairs. Generally, the different toughness properties of each adhesive, and each interface involved in the patch, are assessed through classical fracture mechanics investigations using standardized tests such as End Notched Flexure (ENF) (ASTM D7905 [1]) or Double Cantilever Beam (DCB) (ASTM D5528 [2]) tests, and simple theories based on linear elastic fracture mechanics. Several methods are commonly used to compute the critical toughness from those tests, whether in mode I, II or mixed mode: for instance, the Compliance Calibration Method, or the Modified Beam Theory Method as resumed by Da Silva [3]. Each of these methods requires normally whether a large number of samples, or to carry out the required crack length measurement during the whole test period. Two standard test methods are currently being used to monitor the crack: visual inspection (ASTM D7905 and ASTM D5528) and digital image correlation (DIC). These two methods can ensure good measurement accuracy if the crack propagates slowly with a straight front perpendicular to the direction of propagation.

In addition, given that the measurement is made on the flank of the specimen, the crack front position can be measured with an error of several millimetres. The obtained results accuracy is therefore dependent on the crack shape and on the perpendicularity of the crack front during the test (shown by Meadows [4]). Moreover, in the case of visual inspection, the measurement is highly dependent on the operator.

For these reasons, the use of alternative measurement techniques is required to ensure a precise, robust, with high spatial resolution and easy to use, crack front measurement. High spatial resolution distributed optical fiber may provide such an alternative. This kind of sensor has already been used with success for Carbon Fiber Reinforced Polymer (CFRP) crack propagation monitoring by Meadows [4] or Bernasconi [5] (with Bragg's sensors in [5] having much lower spatial resolution). For those applications, the fiber was embedded in one ply of the composite in small thickness sample. Our study undertakes to extend the fields of application of such sensors to the field of adhesive joint, for less advantageous cases (thicker samples and bonding of the fiber on the surface of the joint) and with more recent optical fiber technology (high spatial resolution continuous optical fiber). The idea is to study if these optical fibers can be able to follow the crack front propagation with a simple application on the surface of the sample, which require a much simpler manufacturing protocol and lead to a more common application.

The distributed optical fiber sensors can be used to collect strain measurements along the entire length of the fiber. The capacity to obtain in real time nearly continuous data such as strain, pressure or even temperature in materials, with only one optical fiber of length up to ten meters is really attractive. In addition, the relatively small size of optical fiber allows them to be integrated directly in an assembly (as shown by Guo [6]) as a bonded or composite structure (described by Murayama [7]) with limited impact on the overall resistance. A tunable frequency laser is used to measure the unique backscattering light along the fiber. Physical changes (as temperature or displacement) induce the fiber to contract or expand changing the Rayleigh pattern and the backscattering. To convert these changes into physical values, the measurement signal, returned from the fiber, is divided into small areas (≥ 1 mm). This is particularly interesting to follow propagation of physical phenomenon with good spatial resolution. In the field of application of this study, in the case of steel-to-steel ENF and DCB tests, to the authors knowledge, no attempt has been made to use such technology to monitor crack propagation and thus to improve the critical toughness determinations while discarding the normally high number of samples required.

The present paper describes the experiments that were carried out for the ENF and DCB test to allow a faithful characterization of the interface investigating the potentialities offered by continuous optical fiber monitoring. Firstly, the use of optical fiber as a methodology to monitor crack propagation is developed. After some theoretical explanations, the led experimental investigations are being described: the studied samples and test bed geometries, the different monitoring systems used in this analysis (distributed optical fiber sensor and digital image correlation) and their locations. Then, visual validation of the crack propagation monitoring is presented and discussed, Next, for the ENF and DCB, the optical fiber measurements and their analysis is made. The ability of the fiber to follow (depending of their position) the crack front position and propagation are compared. Precisely, two optical fiber positions (on top or inside the sample) are used in this study using the previously developed analytical expressions. Finally, the obtained crack data is used to compute and compare critical toughnesses in mode I and II, G_{IC} and G_{IIC} using standard and non-standard methods as described by Girolamo [8] or Leffler [9].

2. Optical fiber crack front measurement methodologies

To study the crack front position extracted from strain curves obtained with the optical fibers for each test, a correct understanding of the strain state on the surface of the tested samples is required for both, ENF and DCB test.

2.1. Theorical ENF crack front measurement

The ENF test corresponds to a 3-point bending tests (Figure 1). Upstream from the crack front, the ENF sample has a thickness $2 * h_s + h_a$ (with h_s and h_a, the steel and adhesive thickness respectively), while downstream from the crack front, the sample is equivalent to the superposition of two beams of thickness h_s (neglecting the friction). Then, following the beam theory, the strains in surface of the sample, ε_{xx1} and ε_{xx2}, respectively upstream and downstream from the crack front, follows the equations (1) and (3). ε_{xx2} is maximal at the junction of the bonded and un-bonded beams which correspond to the location of the crack tip, while ε_{xx1} is maximal at the load application point. The local maximum at the junction of ε_{xx1} and ε_{xx2} is set as the position of the crack front (figure 1).
This analysis relies on two important assumptions:
  * The supposed plasticity/damaged inside the bondline (Fracture Process Zone size) remain limited and has limited impact on the strain measurement obtained with the optical fibers
  * The crack front is far enough from the load application to ensure no interference.

$$\varepsilon_{xx2} = -\frac{M_{fz}(x)}{E_s I_{hz2}} \frac{h_s}{2} \quad \text{(Figure 1)} \tag{1}$$

With M_{fz} the bending moment, E_s the steel Young's modulus, h_s the steel plate thickness and I_{hz1} the moment of inertia of the steel plate given by:

$$I_{hz2} = \frac{2B{h_s}^3}{12} \tag{2}$$

With B the width of the steel plate.

$$\varepsilon_{xx1} = -\frac{M_{fz}(x)}{E I_{hz1}} \left(\frac{h_a}{2} + h_s\right) \quad \text{(Figure 1)} \tag{3}$$

With h_a the adhesive thickness and $E I_{hz2}$ the equivalent stiffness of the bonded plate given by:

$$EI_{hz1} = \frac{E_s B}{12}((h_a + 2h_s)^3 - (h_a)^3) + \frac{E_a B}{12} h_a{}^3 \qquad (4)$$

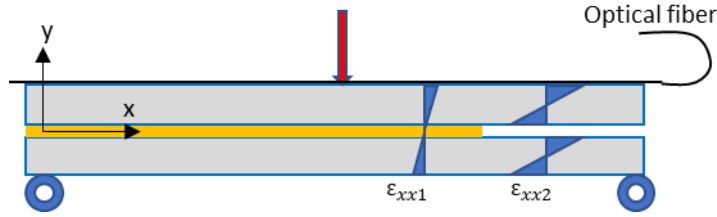With E_a the adhesive Young's modulus.

Figure 1: Scheme representing strain profiles for two characteristic cross-sections into the ENF sample during loading

Using those equations, it appears that the position of the crack tip may be related to the position where the strain value measured by the optical fiber will adopt a local maximum value. Strain monitoring on top or bottom surface or inside the joint, and the determination of local maximum value's position may therefore provide a way to monitor crack propagation for this case.

2.2. Theorical DCB crack front measurement

The same analysis, as the ENF test, has been performed with the DCB test on top and bottom surfaces. The geometry of the DCB test is reminded in figure 2. Following the equation (5), the maximal local rotation variation $(\frac{d\omega}{dx})$ of the samples is supposed to occur closed to the crack tip, and thus the position of the maximal strain measured at the surface of the adherent should correspond to the position of the crack front.

$$\varepsilon_{xx1} = \frac{d\omega}{dx} = -\frac{M_{fz}(x)}{E_s I_{hz1}} \frac{h_s}{2} \quad \text{(Figure 2)} \qquad (5)$$
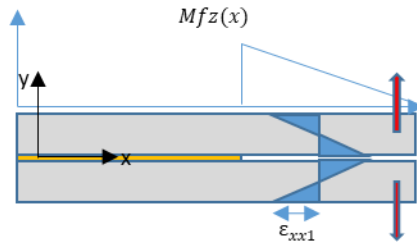

Figure 2: Strain into the DCB sample during loading

By determining the maximum value of the strain profile measurement obtained with an optical positioned on bottom or top surface of the specimen, the crack front position can be estimated.

2.3. Experimental investigations

For the experimental investigations, both geometries were settled according to ASTM D7905 standard (ENF test) that provides three standard test procedures to characterize the interlaminar fracture toughness in mode II for unidirectional carbon fiber reinforced polymer (CFRP) materials. The standard samples geometries proposed for unidirectional CFRP laminate, have been up-scaled by a factor 2 and the substrates has been changed by steel plates. The dimensions of the samples (500x50x11mm) are

similar for ENF and DCB tests as shown in Figure 3. It is supposed that to obtain critical toughness as conservative as possible, the crack measurement should be carried out in the center of the sample (the plain strain state in the sample will imply the measurement of a longer crack length than on the border). This must be the case either with straight (angled or not) crack front or non-straight crack front (angled or not). Considering this issue, it was decided in our study to increase the width of the specimens (increase the plane strain/plane stress ratio) in order to increase the conservatism of the measurement. The initial crack was done using soap and a Teflon insert placed between the steel plates (initial crack length set to 85mm).

The specimens were made with S355 rolled steel plate (thickness 5 mm, width 50mm, with ~1mm radius edge fillet) cut to the right length. The bonding operation was processed as follows: a 1mm steel plate was inserted at each end of the sample (out of the bonded zone), the resin was applied with a 2-5mm thickness on the 2 surfaces of the bonding, then the samples were assembled and pressured between two 10mm steel plates up to the point where the joint was 1mm thick (the two adherents being in contact with the 1mm steel inserts). Thickness measurements were made at several locations of the sample after the test to ensure that there was no larg variation (<10%) of the thickness of the bondline along the length of the sample.

The adhesive is a cold curing epoxy (silicon toughened epoxy - Sikadur® 30). The main properties of the adhesive are given in Table 1 (from technical data sheet). Steel surfaces were sanded and degreased prior to bonding. The sample was then cured at 20°C during seven days before being tested.

Table 1. Sikadur® 30 mechanical properties in tension

Young modulus	Tensile strength	Strain at failure
11 GPa	25 MPa	1%

The test fixtures (Figure 3a and 3b) have also been adapted to the new samples geometry (compared to the one proposed by the ASTM D7905 and D5528). The increase in length and width implied increasing the overall size of the assembly (Figure 4a and 4b) as proposed by Tsokanas [10]. This increase, especially in width, is motivated by the fact that the measurement of the critical toughness is related to the crack propagation (propagation speed, and load at brake) which is also related to the stress state in the sample during the loading. The adopted geometrical values allow obtaining mainly plane strain state inside the joint. Similarly, the initial crack length has been increased compared to the ASTM standard, to ensure that the crack propagation remains under control. Too little initial crack length can indeed tend to uncontrolled crack propagation for the ENF test as shown by Allix [11]. The load application is carried out according to (ASTM D7905) at a constant speed of 2 mm/min for each test.
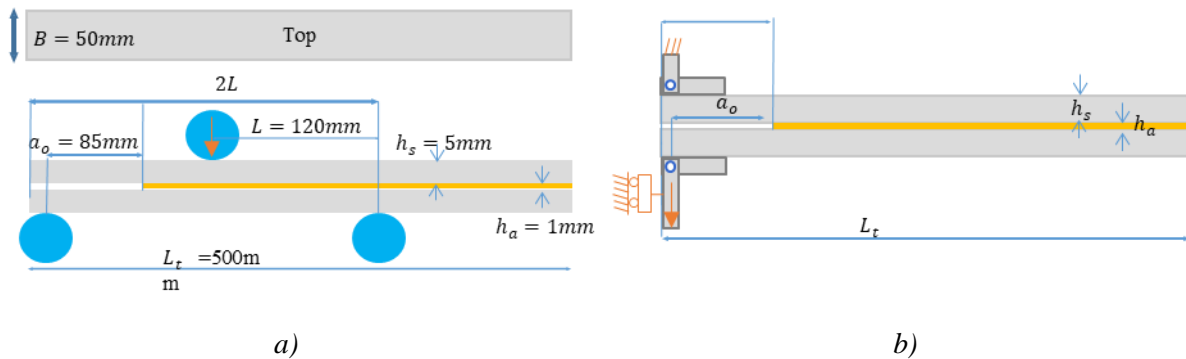

Figure 3. a) ENF Test configuration, b) DCB Test configuration.
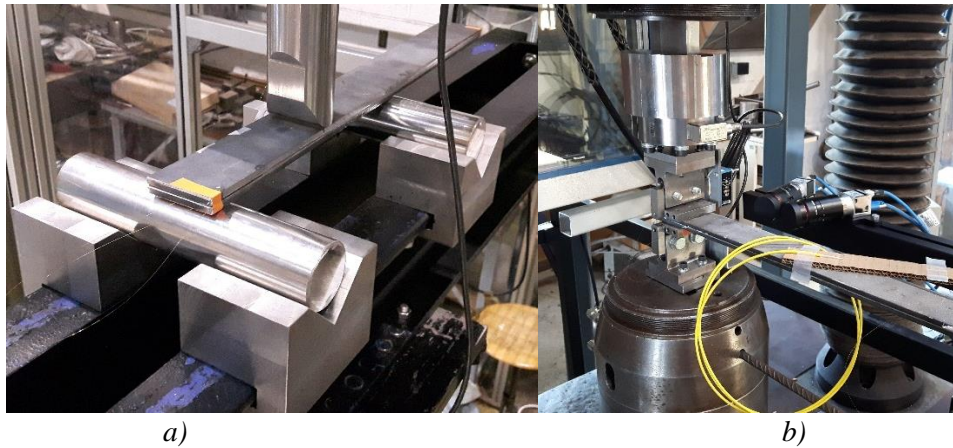
a)	*b)*

Figure 4. a) Photo of the ENF sample and test bed, b) Photo of the DCB sample and test bed.

Applied force and displacements are monitored during the whole test using a 5kN load cell (precision $\pm$ 0.145%) and the laser displacement sensor (precision 10µm). In addition, two monitoring methods are used: continuous optical fiber and digital image correlation.

2.3.1. Digital image correlation

The optical set-up used was, two Basler acA2440-75um cameras (5 Mpx sensor), with two 50mm Kowa LR1015WM52 lenses with a stereo angle of 15 degrees, placed at a distance of around $30 \pm 1cm$ of the sample. The acquisition rate was set at 5Hz. A black and white speckle has been deposited on the test specimen by non-homogeneous spraying of paint in three successive layers (white / black / white) with an approximative pattern size of (visually obtained) of around 0.2mm. A commercial system (Correli^{STC} by Corelli Solution) was used to carry out digital image stereo-correlation on one of the two flanks where the border of the crack front is visible for both tests (DCB and ENF).

The cameras were adjusted following the Corelli$^{©}$ software procedure brightness / sharpness / calibration / synchronization) (see Figure 5). The position of the cameras (distance to the samples) was settled in order to monitor a region of interest (ROI) with a size of 6cm x 2cm for the ENF test and of 3cm x 1cm for the DCB test around the initial crack location. For this application, the used mesh (step size) was 32 pixels x 32 pixels (0.5mm). The subset size was set to 32x32 pixels with Q4 elements. The choice of the resolution has been made following the recommendation of the Correli software speckling analysis tool that proposes the best mesh size compromise between spatial resolution and measurement accuracy. The local displacement measurement resolution is 5µm
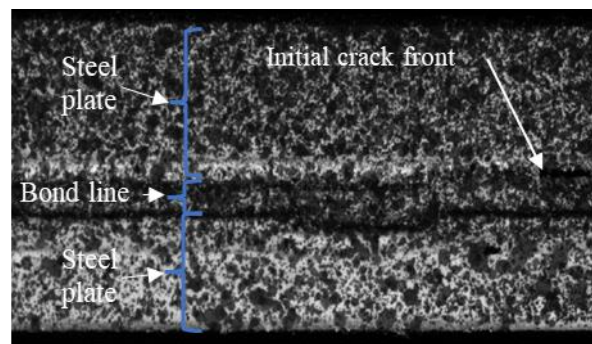

Figure 5. Example of speckle and initial crack,

2.3.2. Continuous optical fiber

The distributed optical fiber sensor system used for the experiments is a Luna ODiSI-B which is based on the measurements of the Rayleigh backscattering of light in the core of the optical fiber by an OFDR (Optical Frequency Domain Reflectometer) system. It allows strain measurement along a fiber up to 10m long, with maximal spatial resolution of 0.6mm (overlapping length) and gauge length of 1.2mm as described in figure 6. It was set at a frequency of 12 Hz, recording the strain during the whole period test, and all along the bonded optical fiber. The recorded noise before the test was +/- 20 µstrain.
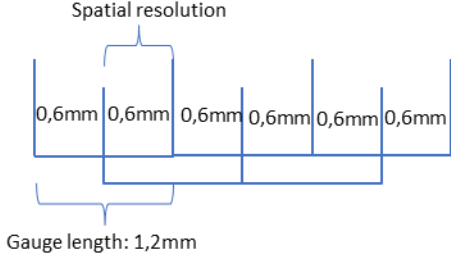

Figure 6. Optical fiber gauge length and spatial resolution

For our test specimens, a 150µm-diameter optical fiber with polyimide coating was bonded in several locations as shown in Figure 7a:
- On the test specimen upper surface, in the center, with Araldite 2014-2 adhesive.
- Inside the bond line, in the center, with the adhesive Sikadur 30.

The disposal of the sample for the test was made in such a way that the exterior optical fiber was underneath the sample (and was under traction during the ENF test). A photo of the overall test setting (for ENF situation) with both local measurement methods is given in Figure 7b.
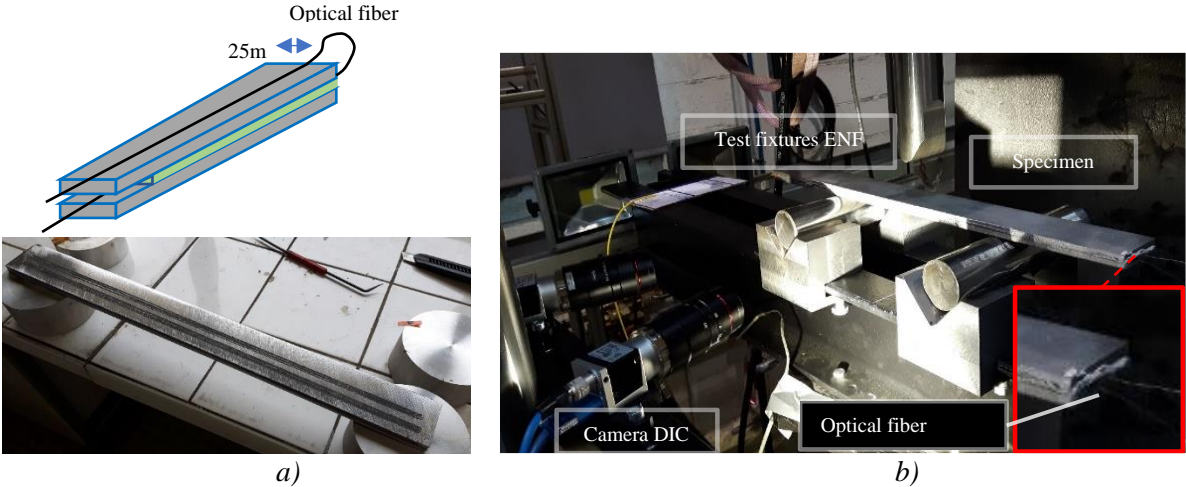

Figure 7. a) Position of the optical fiber and example of optical fiber application on a specimen, b) ENF specimen, instrumentation, test fixtures.

2.4. Experimental validation of the optical fiber crack measurement

To validate the theorical approach exposed in chapter 2.1 and 2.2. A Mixed Mode Bending (MMB) test was conducted. This test was chosen as validation because of his behavior similar to the combination of an ENF and DCB test. The sample is the same and the crack front position was monitored with the exterior optical fiber following the same analysis as the one used for the ENF and DCB tests (position of the local strain peak). The resulting crack monitoring is visible in the Figure 8a. After the end of the test a dye penetrant was used. The area between the initial crack front and the final crack front is colored

by the product, to mark the cracked area of the sample. The measurement of the length of this area at the middle of the sample is set as the crack length at the end of the test as visible in the figure 8b.
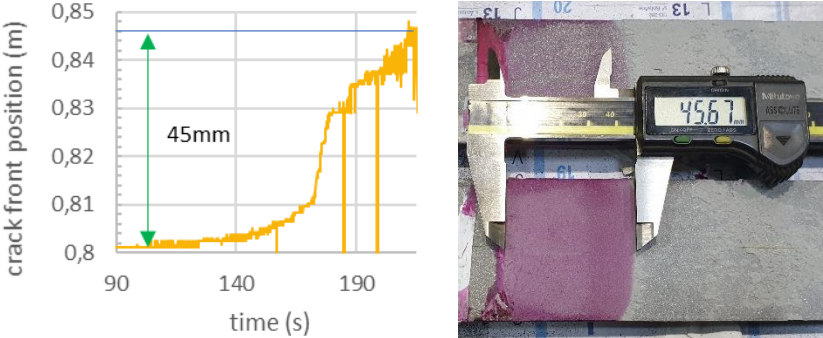

Figure 8: a) Crack propagation measured with the exterior optical fiber. b) Visual measurement of the crack length at the end of the test.

The results shows that the final crack length prediction of the optical fiber is 45 ± 1 mm which is very close the the value obtained experimentally (45.67 mm). This result seems to confirm the assumption made in the chapter 2.1 and 2.2. Thus, if the strain peak is well defined (strain > ~500µm/m), and the noise level of the optical fiber is low enough ($\pm 20 \ \mu m/m$ in this case) the exterior fiber can be used with good confidence as a measurement method of the crack front position. Furthermore, the resulting crack front shape showed that the embedded optical fiber had no impact on the crack front shape that remains straight in the center of the samples. Therefore, it does not seem to influence the crack length measurement and so, the critical toughness measurement. The interest of measuring crack length in the middle of the joint is also highlighted as it can be observed that the crack front is not straight and not perpendicular on the edges where visual inspection and DIC are carried out, as shown in figure 9.

Figure 9: crack length measurement at the border of the sample.

In this case, the maximal difference between the crack front position at the center of the sample and on the edges is 4.5 mm which seems to be important in regards with the studied propagation distance of 45mm.

3. ENF experimental results analysis
3.1. Critical toughness computation method

This chapter describes three computation methods commonly used to obtain the mode II critical toughness. The first one is the Compliance Calibration Method (CCM), as Described by Banea [12].

During the test, the load P, applied displacement δ and crack length a are recorded in order to calculate the strain energy release rate using the Irwin-Kies equation described by Kanninen [13]:

$$G_{II} = \frac{P^2}{2B}\frac{dC}{da} \tag{6}$$

With, B the width of the specimen, C= δ/P the compliance.

For the ENF test, it has been proposed by Davies [14] to use equation (7) to express the compliance as a cubic function of the crack length a, as:

$$C = D + ma^3 \tag{7}$$

With D and m are constant values.

G_{IIC} can then be expressed as:

$$G_{II,Dav} = \frac{3P^2\,ma^2}{2B} \tag{8}$$

This approach requires calibration of compliance as a cubic function of crack length, normally done with multiple samples (at least 3) with different initial crack lengths. In our case, the authors made the hypothesis that it can be directly obtained by monitoring the crack propagation curve measured with the optical fiber during the test for one sample, which reduce the number of test required for the calibration of C to only one. This approximation being highly dependent on the crack length measurement, especially for limited crack propagation length such as in ENF test, it can lead to error if the crack front is not monitored properly, or if the initial crack front is not well defined. Measuring the crack length remain difficult to do, the propagation can be fast and location of the crack front is depending on the visual acuity of the operator

The ASTM standard D7905 proposes another approach following the compliance calibration. It does not need to monitor the crack propagation, but requires a higher number of samples and tests with different initial crack front lengths to establish the relation $C=f(a)$, which is regressed using the same cubic function as in previous paragraph. This approach assumes that crack propagation only takes place when the force has reached its peak P_{max} the load corresponding to crack onset, leading to the equation (9). This approach does not take into account the need for a minimal crack propagation length to ensure the stabilization of the toughness to its maximal value plateau as expressed by Chaves [15].

$$G_{IIC,ASTM} = \frac{3P_{max}^2\,ma_0^2}{2B} \tag{9}$$

The above methods can only be used in cases when linear elastic fracture mechanics (LEFM) theory can be applied, which assumes that there is limited material non-linearity in the adhesive. Therefore, data reduction techniques neglect the impact of the process zone upstream of the crack front. This can lead to inaccurate G_{IIc} for materials that develop a rather large process zone compared to the overall size of the samples. The J-integral is a technique used for calculating the fracture energy for problems where the assumptions of the LEFM are no longer valid. It is defined by a contour integral whose value is equal to the energy release rate. Rice [16] has shown that for monotonic loading, with crack propagation occurring in homogenous material, the J-integral is path independent and its value is equal to the energy released during the damage process for linear and nonlinear elastic body. Those two properties allow us to select the most convenient path to integrate the stresses and to compute the energy release rate from common tests, as ENF one. Leffler [9] proposed a simplified expression of the J-integral based on

LFEM, taking into account the substrate strain and shear strain in the adhesive (Equation 10) for the ENF test. The first term of this equation corresponds to the classical beam theory considering a rigid adhesive while the second term corresponds to the effect of the flexibility of the adhesive.

$$J_{ENF} = \frac{9}{16}\frac{(Pa_0)^2}{E h_s{}^3 B^2} + \frac{3\delta_s}{8 h_s B} \qquad (10)$$

With P the load, a_0 the initial crack length, δ_s the local sliding (see Figure 10), E the adherent Young's modulus, h_s the adherent thickness and B the sample width.

This simplified equation has shown good results in several studies, as shown in [8] where critical toughness was obtained for multi-layered composites double lap joint using this expression of J_{ENF}. To be applied, a long enough distance between the crack tip and the loading point must be ensured to avoid any impact of the local stress concentration of the application point in the bondline.
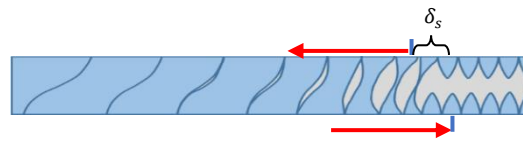

Figure 10. ENF local sliding at the crack front.

3.2. Load displacement curve

The obtained load-displacement curve for the ENF test is shown in Figure 11. Three stages can be observed. The first one is a linear elastic stage up to point A. Once the load exceeds the point of proportional limit, damage appears in the bondline, extends and forms the fracture process zone (FPZ) which leads to a slope decrease, and an increase of the compliance. When the FPZ is fully developed and the crack propagation begins, the load-displacement curve reaches its maximum point (point B). The crack propagation is assumed to occur up to the local minimum after the first load decrease (between B and C). This corresponds to times: t_B=58s to t_C=68s. Consequently, the upcoming analysis will be focused on the results computed between these two times.
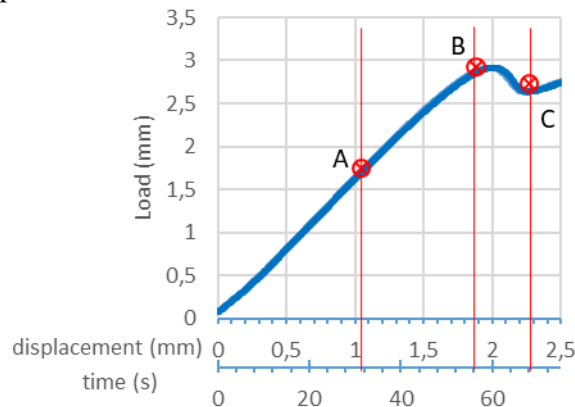

Figure 11. ENF Load displacement curve.

3.3. Optical fiber analysis and crack propagation determination
3.3.1. Embedded optical fiber

In Figure 12, the strain profiles measured with the optical fiber inserted inside the bond layer at different time before the crack propagation (i.e. before point B: $t<t_B$), presents an initial peak value which is supposed to correspond to the position of the initial crack front at x=0.087m (made during the fabrication by inserting Teflon tapes). During the whole test period, this initial strain jump remains at the initial crack front position, but the strain profile is then modified along the joint. The experimental results show a strain plateau with a length of 1mm at the beginning of the non-linearity (at point A) on the Figure 11. This plateau increases up to 14mm at the moment of the initial crack propagation (at point B). This is assumed to be linked to damage near the crack tip before its propagation, and could thus be used as a measurement of the fracture process zone (FPZ) length. In our case, the zone length is at its maximum (figure 12 and 13) with a length of around 1cm, see curve at time t = 53s and t = 60s. After the initial crack propagation (Figure 13), no really visible indication is seen with the fiber measurement regarding the crack front position during the test. This result seems to indicate an incapacity to follow the crack propagation using the embedded optical fiber and with a simple analysis of the strain state inside the bondline.
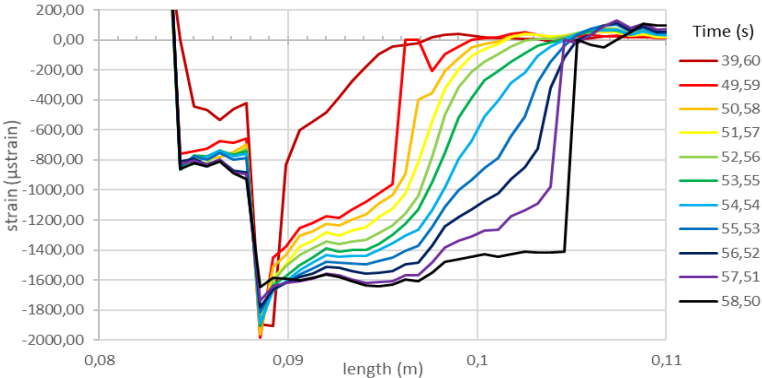

Figure 12. Embedded distributed optical fiber strain measurements before 58s.
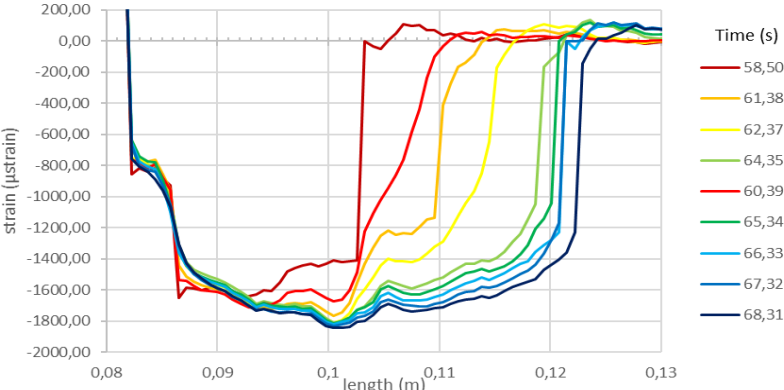

Figure 13. Embedded distributed optical fiber strain measurements after 58s.

3.3.2. Exterior optical fiber

Figure 14 presents the obtained strain measurements along the length of the sample for the exterior optical fiber placed at mid-width of the sample during the crack propagation, compare the analytical prediction. Each curve corresponds to a different time. It can be observed that a maximum strain value can be indeed measured and that the position, for which this maximum strain value is obtained, evolves along the test.
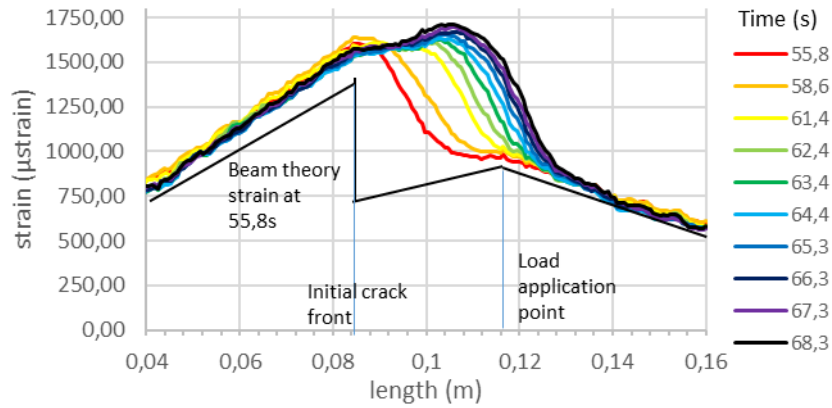
Figure 14. Exterior optical fiber distributed strain measurements between time 55.8s and 68.3s.

The position around 0.086 m corresponds to the initial crack length. The maximal values of the optical fiber strain measurement versus the axial length for different times between t_B and t_C is plotted in Figure 15a. A shift of the maximum of the curve to the right can be observed, indicating a displacement of the crack tip. The study of the displacement of this peak is then post-treated to obtain the crack propagation. The resulting curve (Figure 15b) shows that the main crack propagation occurs between 62 and 64 seconds. This confirms the fact that the global crack propagation occurs between B and C. A smoothing of the data with the use of moving average has been made to reduce the raw crack front computation noise (Figure 15b) (each raw data value, is converted to average of the 5 data points centered on the original value).

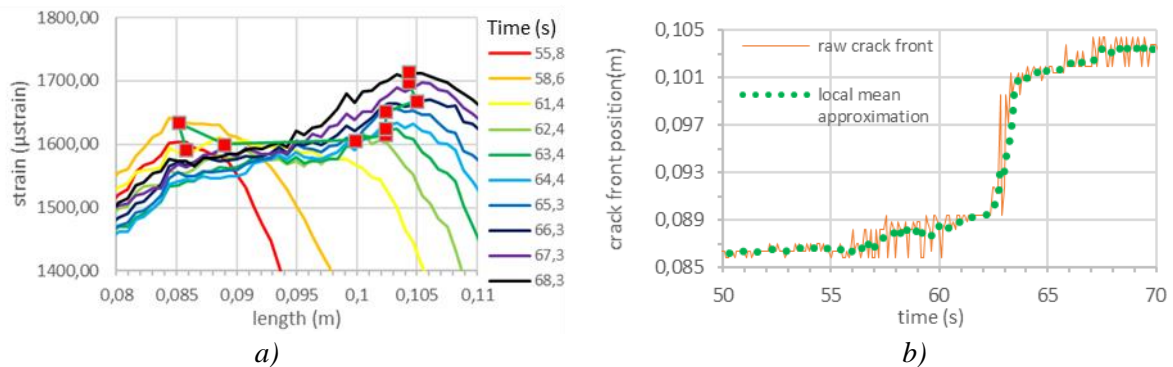a)   b)

Figure 15. a) Locations of the maximum position of optical fiber strain measurement. b) Crack propagation curve for the ENF test - data processing via local mean approximation.

3.4. Strain Energy release rate computation

The following curves represent the results of calculations obtained using Equations (6) and (7). Using the obtained crack propagation curve and the Davies formula with the obtained parameter *m* (Figure 16a), it gives the curve in Figure 16b, with a pseudo-stabilization around the value 0.88 ± 0.04 kJ/m².
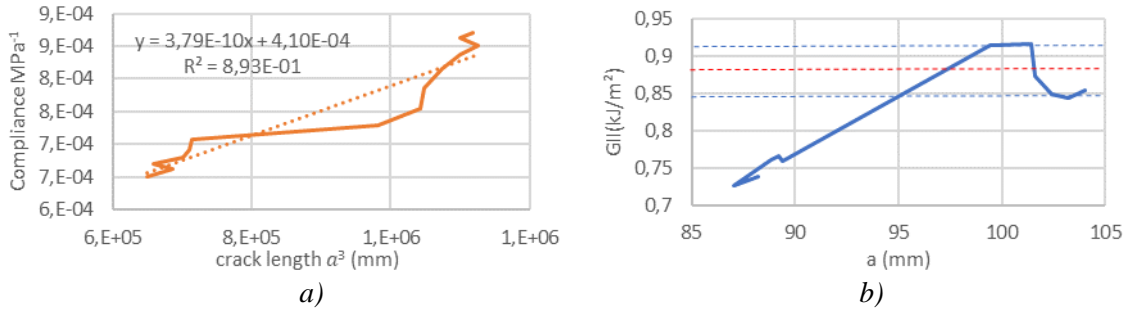
Figure 16. a) Cubic $C = f(a^3)$ approximation, and linear regression, b) GII$_C$ computation with Davies approximation.

Likewise, the use of equation (8) with the values P_{max}= 2900N, a_0= 85mm (obtained with the embedded optical fiber), and m=3.79 10^{-10} Mpa/mm³ (obtained with exterior optical fiber in the previous chapter) allows obtaining the value G_{IIC} = 0.71 kJ/m². This value is lower than the one obtained with the CCM computation. In addition, the initial crack front is artificially created by the Teflon insert, which is not a perfect crack front. The previous methods can only be used in cases when linear elastic fracture mechanics (LEFM) theory can be applied, which assumes that the material is isotropic and linear elastic. Therefore, data reduction techniques neglect the impact of the process zone upstream of the crack front. This can lead to inaccurate G_{IIc} computation for materials that develop a rather large process zone compared to the overall size of the samples.

To determine J$_{ENF}$ values, the DIC system was used to measure the displacement fields (local sliding) at crack tip (initial crack front) on the profile of the specimens. Figure 17a shows the size and local displacement measurement performed by the DIC software. The step size is 32x32 pixels, which is equivalent to 0.7x0.7mm on an array of 10x40mm upstream of the crack front. The subset chosen for the displacement measurement were chosen at a distance at least one step away from the bonded zone to avoid any issue caused by the local displacement discontinuity.

The obtained J-integral curve, using Equation (10), is shown in Figure 17b. The toughness value at stabilization is equal to G_{IIC} = 0.8 kJ/m² which occurred at the time where the crack propagation occurs, at t=58s (Figure 11). It must be noted that the effect of the second term of Equation (10) proved to be non-negligible (~70% first term and 30% second term of J_{ENF} at stabilisation) in our case following the local sliding measured using the DIC measurement.
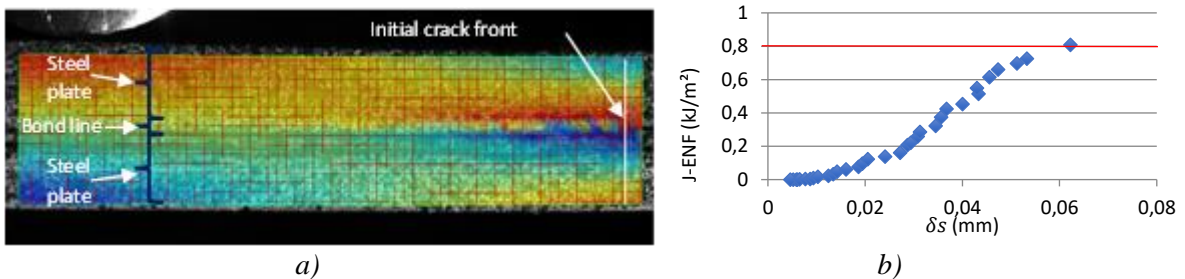

Figure 17. a) Stereo-correlation data analysis for horizontal displacement, b) ENF J-integral vs horizontal displacement jump.

All the obtained results (critical toughness) with the three presented methods are given in Table 2. It can be seen that the three values are very close, indicating consistency of the three approaches. It can be noted that the value determined using the ASTM approach is 20% lower. When taking into account the maximum force value, one indeed neglects the need for a minimum crack propagation to have a maximal stabilized critical energy release rate. This tends to underestimate the correct crack length. In addition,

these values are similar to other values found in the literature for mode II tests on toughened epoxy such as the ones obtained by Dimoka [17] or on standard epoxy as described by Chaves [15] or Ashby [18].

Table 2: Determination of G_{IIC} with the three studied methods in comparison with the state of the art

Model	G_{IIC} (kJ/m²)
CCM [14] with crack propagation measurement by optical fiber	0.88 ± 0.04
Standard characterization without crack propagation monitoring, [1]	0.71
J-integral method [9]	0.8
Chaves [15]	0.7 - 0.9
Ashby [18]	0.1-5
Dimoka [17]	0.5 - 0.9

4. DCB experimental results analysis
4.1. Critical toughness computation method

The ASTM D7905 proposes to use the Beam Theory Method (BTM) which is a direct application of the beam theory, for the computation of the critical energy release rate G_{Ic}. A perfectly cantilever built-in beam is considered (this assumption is made directly at the crack front) leading to the Equation (11).

$$G_{Ic\,BTM} = \frac{3P\delta}{2Ba} \tag{11}$$

With P the load, B the width, δ the displacement at the load application point and a the crack length. This equation slightly overestimates G_{Ic} as the beams are generally not perfectly built-in. Thus, a new equation, introducing a compensation factor [2], can be used taking into account these rotations (Modified Beam Theory Method, see Equation 12).

$$G_{Ic\,MBTM} = \frac{3P\delta}{2B(a + |\Delta|)} \tag{12}$$

With P the load, B the width, δ the load application point displacement, a the crack length computed using the exterior optical fiber and Δ a compensation factor for the rotation of the adherent upstream of the crack front which must be experimentally determined by generating a least square fitting of the compliance curve ($C^{1/3}$) versus the crack length.

The J-integral approach for the DCB test, Proposed by Högberg [19], was also used to compare the results with the ASTM method. The digital image correlation system was used to measure the displacement fields at crack tip (initial crack front) on the side of the specimens. For the DCB configuration, it is necessary to determine the local opening, δ_n, and the contribution of the local rotation of the upper θ_{sup} and the lower θ_{inf} adherent (see Figure 18).
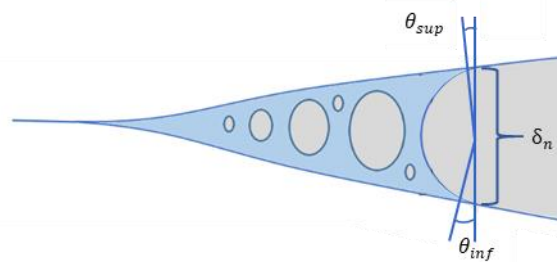

Figure 18: Local opening and local rotation at the crack front.

The analytical expression of the J-integral proposed used for DCB test (Equation 13) is based on LEFM. This expression was used in several studies, such as in [11] for cohesive law calibration. As for the ENF test, it must be specified that in the equation (13), the first term corresponds to the beam theory considering a rigid adhesive while the second term corresponds to the effect of the flexibility of the adhesive and the local rotation of the adherent.

$$J_{DCB} = \frac{12(Pa_0)^2}{Eb^2h^3} + \frac{P}{b}|\theta_{sup} - \theta_{inf}| \tag{13}$$

4.2. Load displacement curve

The Figure 19 shows the load-displacement curve of the DCB test. As for the ENF, three stages can be observed. Once the load exceeds the point of proportional limit (Point D), damage in the bondline extends and forms the fracture process zone (FPZ) which leads to an increase of the compliance and a deviation of the curve. When the FPZ is fully developed, the load-displacement curve reaches its maximal value (Point E). Beyond the point E, the crack propagates.
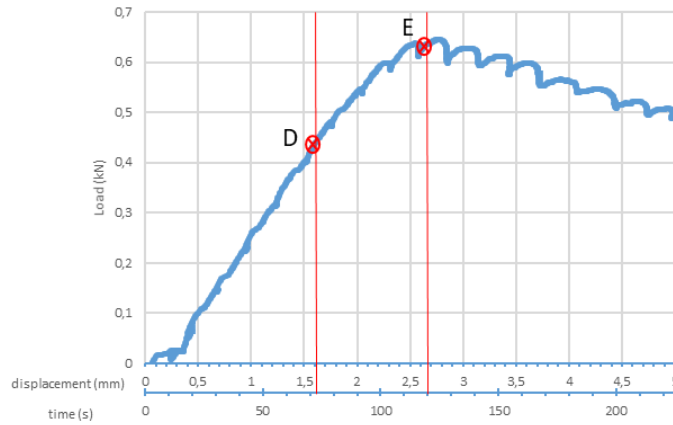

Figure 19: DCB Load displacement curve.

4.3. Optical fiber analysis and crack propagation determination

The Figure 20 presents the measurements with the exterior optical fiber during the crack propagation. Each curve corresponds to a different time.
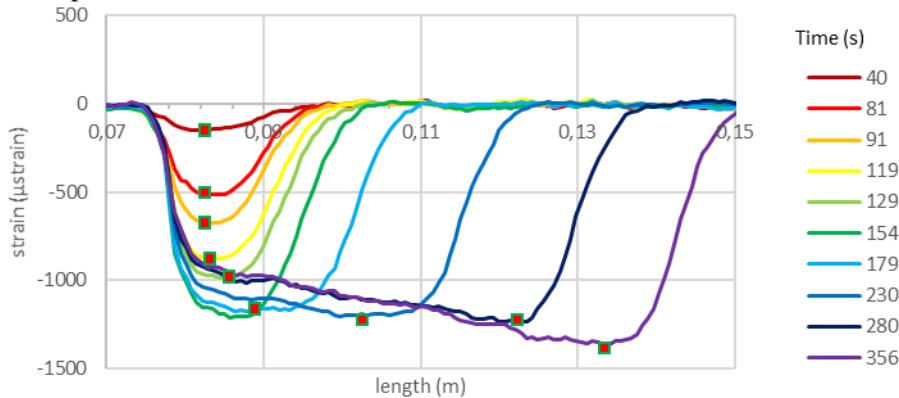

Figure 20: DCB exterior optical fiber continuous strain measurements along lap length for different times.

The study of the position of the peak (red dots in Figure 20) is used to monitor the crack propagation. It is verified that ~0.085 m corresponds to the initial crack length. For the curves corresponding to a time measurement between $t_D = 72s$ and $t_E=120s$, we can observe a slight shift of the maximum of the curve (as for the ENF) which is supposed to be related to the process zone development (micro-cracking and/or damage). The figure 20 shows that the main crack propagation (macro-crack) occurs after the time t_E. A post processing of the data has been made to reduce the raw crack front computation noise (moving average) as shown in figure 21.
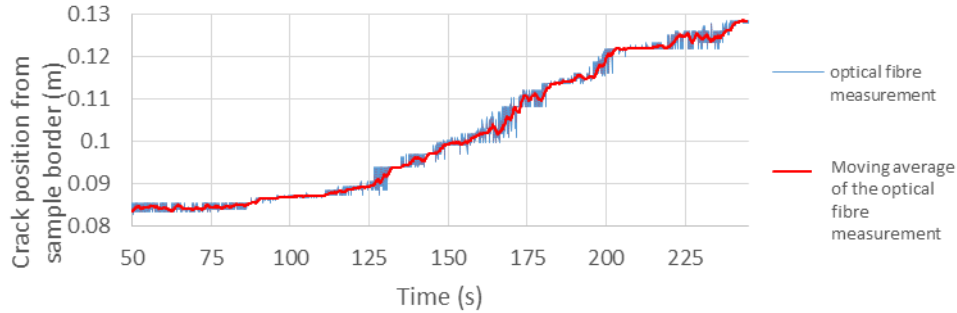

Figure 21. Crack propagation curve for the DCB test - data processing via local mean approximation.

4.4. Strain Energy release rate computation

The first computation method, based on Equation (12) proposed by the ASTM standard, require to obtain initially Δ which in our case, is equal to 3.5mm following the calculation proposed by ASTM D5528. The result of the application of Equation (12) is given in Figure 22.
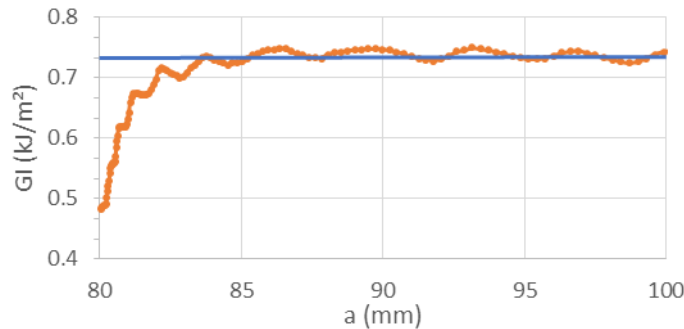

Figure 22: Computation of G_{Ic} with MBT method.

The resulting curve shows that after an initial crack propagation of 5 mm, the computation of the critical toughness stabilizes around the value $G_{Ic} = 0.73$ kJ/m².

To determine J_{DCB} values, the DIC system was used to measure the rotation and displacement fields (local rotation) at crack tip (initial crack front) on the profile of the specimens. Figure 23a shows the step mesh and local displacement interpolated by the DIC software. To do this, the DIC technique was used with a step size of 32x32 pixels, which is equivalent to 0.4x0.4mm on an array of 10x18mm upstream of the crack front. The local opening δ_n, can be directly determined using the digital image correlation data. $|\theta_{sup} - \theta_{inf}|$ is determined using longitudinal displacement measurements for two sets of points above and under the bond line from digital image correlation measurements (Points A, B, C and D on Figure 23a). These points (as for the ENF test) were chosen at a distance at least one step away from the bonded zone to avoid any issue caused by the local displacement discontinuity. The resulting J-integral curve (equation 13) is shown in Figure 23b.
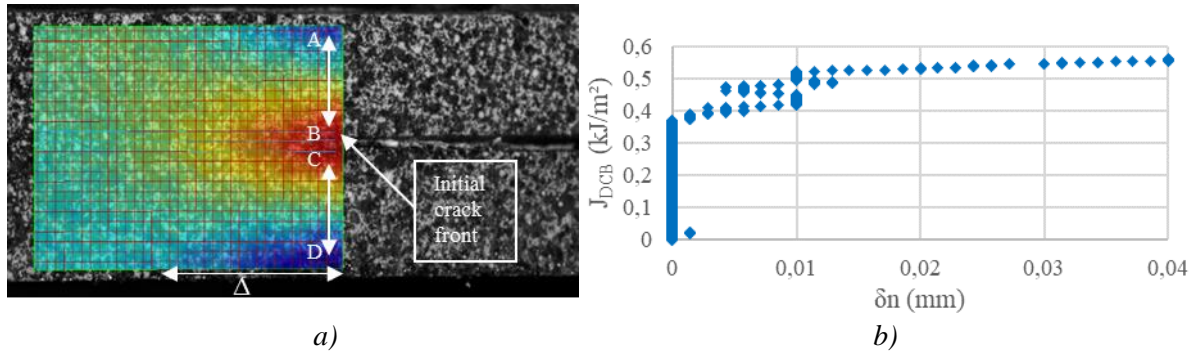
Figure 23: a) Local horizontal translation map just before the crack propagation upstream of the crack tip, b) J-integral curve vs local displacement.

The results of the DCB mode I critical toughness obtained for the different approaches are summarized in the Table 3. A difference of 23% was found between the ASTM and Högberg [19] methods. This is higher than the one obtained for the ENF test. This difference is supposed to be related to the overestimation made by the MBT theory on the supposed perfectly built-in beam at the crack tips, which is not in agreement with the DIC measurements.

Table 3: Result table of the computation of G_{IC} for the MBT and DIC methods

Model	G_{IC} (kJ/m²)
MBT with crack propagation monitoring by optical fiber [2]	0.73
J-integral [19]	0.56
Dimoka [17]	0.4 – 0.9
Kouno [20]	0.15 – 0.25
Ameli [21]	0.3 – 0.4

The obtained DCB results are relatively similar to the ENF ones, which is not common, as the mode II critical toughness is generally described as higher than the mode I for carbon fiber reinforced polymer (CFRP) with epoxy or epoxy in adhesive joints, as shown by Kouno [20] and Ameli [21].

It is to be precised, that the obtained values remain in adequacy with the results exposed for highly toughened epoxy adhesive in [17,20,21]. The overall critical toughness results obtained with the different methods of this study are resumed in figure 24.
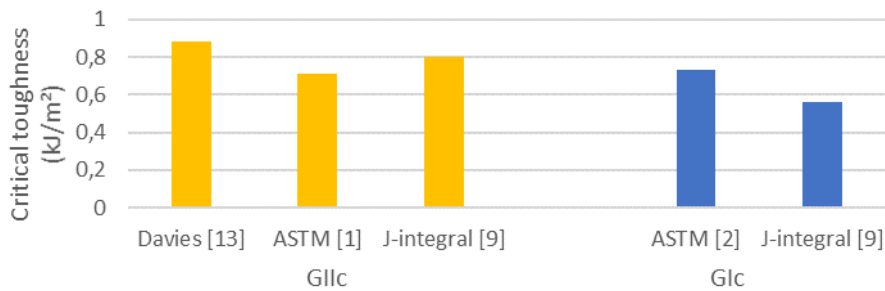

Figure 24: Critical toughness results

5. Conclusion

This study investigated the use of continuous optical fiber to measure the crack propagation and determine the critical toughness for steel to steel adhesively bonded joints in mode I and II (using DCB and ENF test respectively). It was shown that the high spatial resolution and the accurate strain measurement of the used optical fiber can greatly improve the analysis of such investigations. For these tests, the optical fiber being located inside the specimen was not enable to monito crack propagation to while the external fiber proved to give access to consistent crack propagation data during the test.

The central position of the exterior optical fiber is supposed to reduce error in crack front position compared to more commonly used methods such as DIC or visual inspection that are highly dependent on the crack front shape (both those methods are carried out on the side of the sample). In regards with visual inspection, the use of the optical fiber seems more robust and less dependent on the operator. In comparison with DIC, post-processing appears to be easier to carry out and several optical fibers could be used to improve crack propagation monitoring reliability and to study, for specific cases, crack front shapes in the width of the samples. A precise methodology was also validated for ENF and DCB configurations to determine the crack front position using the optical fiber measurements. It must be noted that these results have been obtained with relatively thick steel-to-steel bonded samples. This methodology could be used on other samples with different materials (fiber reinforced composites or metals) or different samples shape. It may even be used for crack monitoring of full size CFRP reinforcement patches. It can also be highlighted that the final procedure does not require, any embedment of the optical fiber simplifying the realization of the samples.

Using simplified hypotheses/assumptions (LEFM) and the obtained data, the critical toughness of the bonded joint for both mode I and II determined. For ENF test, the obtained results considering three different theories are very close, indicating a good consistency of the different approaches. In addition, it was shown that the inner optical fiber allows to monitor the strain state inside the bondline and to give information on the process zone length during the ENF test. For the DCB test, the low level of noise during the measurement allowed to easily obtain the crack length using the exterior optical fiber. The two obtained critical energy release rate are quite similar, with a LEFM prediction higher than the J-integral one. For both cases, the obtained critical toughness values are closed to the ones obtained in the literature for similar joints indicating a good consistency of the proposed methodology. The results obtained during this work showed that high spatial resolution optical fiber well positioned can be used to monitor accurately the crack propagation during fracture tests.

Additional investigations are currently realized to use such crack monitoring techniques in other mechanical investigations such as full-size carbon fiber reinforcement patch. The analysis of the optical fiber measurement along the process zone will also be further investigated comparing it with the results of Non-Linear Finite Element Models relying on the use of cohesive zone elements.

Bibliography

[1] D7905 Standard test method for determination of the mode II interlaminar fracture toughness of unidirectional fiber-reinforced polymer matrix composites. West Conshohocken, PA: ASTM International. 2014.

[2] D5528-01 Standard Test Method for Mode I Interlaminar Fracture Toughness of Unidirectional Fiber-Reinforced Polymer Matrix Composites West Conshohocken, PA: ASTM International. 2014.

[3] Da Silva L F M, Dillard D A, Blackman B R K, Adams R D. Testing Adhesive Joints, Best Practices. Wiley-VCH. 2012.

[4] Meadows L, Sullivan R, Brown K, Ranatunga V, Vehorn K, Olson, S. Distributed optical sensing in composite laminates. The Journal of Strain Analysis for Engineering Design. 2017;52:410-421.

[5] Bernasconi A, Carboni M, Comolli L. Monitoring of fatigue crack growth in composite adhesively bonded joints using Fiber Bragg Gratings. Procedia Engineering. 2011;10:207-212.

[6] Guo H, Xiao G, Mrad N, Yao J. Fiber Optic Sensors for Structural Health Monitoring of Air Platforms. Sensors. 2011;11:687-705 .

[7] Murayama H, Kageyama K, Uzawa K, Ohara K, Igawa H. Strain monitoring of a single-lap joint with embedded fiber-optic distributed sensors. Structural Health Monitoring. 2011;11:325-344.

[8] Girolamo D, Dávila C, Leone F, Lin S-Y. Cohesive Laws and Progressive Damage Analysis of Composite Bonded Joints, a Combined Numerical/Experimental Approach.56th AIAA/ASCE/AHS/ASC Structures, Structural Dynamics, and Materials Conference. 2015.

[9] Leffler K, Alfredsson S, Stigh U. Shear behavior of adhesive layers. International Journal of Solids and Structures. 2006;44

[10] Tsokanas P, Loutas T, Kostopoulos V, Essa Y, Escalera F. On the design and analysis of interlaminar fracture toughness tests on dissimilar metal-composite adhesive joints with residual thermal stresses. Conference: ECCM18, 18th European Conference on Composite Materials. Athens, Greece. 2018.

[11] Allix O, Ladeveze P, Corigliano A. Damage analysis of interlaminar fracture specimens. Composite Structures. 1995;31:61-74.

[12] Banea M, da Silva L F M. Adhesively bonded joints in composite materials: An overview. Proceedings of the Institution of Mechanical Engineers, Part L: Journal of Materials: Design and Applications. 2009;223(1):1-18.

[13] Kanninen M F, Popelar C H. Advanced Fracture Mechanics. Oxford University Press. 1985.

[14] Davies P. Fracture Mechanics Testing Methods for Polymers, Adhesives and Composites, Chapter: Introduction to delamination fracture of continuous fiber composites, Elsevier Science. 2001;28:271-275.

[15] Chaves F J P. « Fracture Mechanics Applied to the Design of Adhesively Bonded Joints». PhD Thesis of the University of Porto. 2013.

[16] Rice J. A path independent integral and the approximate analysis of strain concentration by notches and cracks. Journal of Applied Mechanics. 1968;35:379-386.

[17] Dimoka P, Kostagiannakopoulou C, Masouras A, Kostopoulos V. Improvement of Interlaminar Fracture Properties of Out of Autoclave Manufactured Carbon Fiber Reinforced Polymers Using Multi-Walled Carbon Nanotubes. World Journal of Mechanics. 2019;09(06):147-162

[18] Ashby. M. Material and process selection charts. Cambridge CB2 1PZ, UK Version 1. 2010

[19] Högberg J L, Sørensen B F, Stigh U. Constitutive behavior of mixed mode loaded adhesive layer, International Journal of Solids and Structures. 2007:44:8335-8354.

[20] Kouno M, Imanaka R, Hino M, Omiya F, Yoshida F. R-curve behavior of adhesively bonded composite joints with highly toughened epoxy adhesive under mixed mode conditions, International Journal of Adhesive and Adhesion. 2020;105.

[21] Ameli A, Papini M, Schroeder J A, Spelt J K. Fracture R-curve characterization of toughened epoxy adhesive. Engineering Fracture Mechanics. 2010;77:521-534.